Brain Stimulation 14 (2021) 290–300

Contents lists available at ScienceDirect

Brain Stimulation

journal homepage: http://www.journals.elsevier.com/brain-stimulation

Transcranial focused ultrasound stimulation with high spatial resolution

Seongyeon Kim [a, 1], Yehhyun Jo [a, 1], Geon Kook [a], Cristina Pasquinelli [b, c], Hyunggug Kim [a], Kipom Kim [d], Hyang-Sook Hoe [d], Youngshik Choe [d], Hyewhon Rhim [e], Axel Thielscher [b, c], Jeongyeon Kim [d, **], Hyunjoo Jenny Lee [a, f, g, *]

[a] School of Electrical Engineering, Korea Advanced Institute of Science and Technology (KAIST), Daejeon, 34141, Republic of Korea
[b] Danish Research Centre for Magnetic Resonance (DRCMR), Centre for Functional and Diagnostic Imaging and Research, Copenhagen University Hospital Hvidovre, Denmark
[c] Center for Magnetic Resonance, Department of Health Technology, Technical University of Denmark, Kgs. Lyngby, Denmark
[d] Korea Brain Research Institute (KBRI), Daegu, 41068, Republic of Korea
[e] Center for Neuroscience, Korea Institute of Science and Technology (KIST), Seoul, 02792, Republic of Korea
[f] KAIST Institute for Health Science and Technology (KIHST), Daejeon, 34141, Republic of Korea
[g] KAIST Institute for NanoCentury (KINC), Daejeon, 34141, Republic of Korea

ARTICLE INFO

Article history:
Received 24 February 2020
Received in revised form
30 November 2020
Accepted 6 January 2021
Available online 12 January 2021

Keywords:
Ultrasound neuromodulation
Brain stimulation
High spatial resolution

ABSTRACT

Background: Low-intensity transcranial focused ultrasound stimulation is a promising candidate for noninvasive brain stimulation and accurate targeting of brain circuits because of its focusing capability and long penetration depth. However, achieving a sufficiently high spatial resolution to target small animal sub-regions is still challenging, especially in the axial direction.
Objective: To achieve high axial resolution, we designed a dual-crossed transducer system that achieved high spatial resolution in the axial direction without complex microfabrication, beamforming circuitry, and signal processing.
Methods: High axial resolution was achieved by crossing two ultrasound beams of commercially available piezoelectric curved transducers at the focal length of each transducer. After implementation of the fixture for the dual-crossed transducer system, three sets of *in vivo* animal experiments were conducted to demonstrate high target specificity of ultrasound neuromodulation using the dual-crossed transducer system ($n = 38$).
Results: The full-width at half maximum (FWHM) focal volume of our dual-crossed transducer system was under 0.52 μm^3. We report a focal diameter in both lateral and axial directions of 1 mm. To demonstrate successful *in vivo* brain stimulation of wild-type mice, we observed the movement of the forepaws. In addition, we targeted the habenula and verified the high spatial specificity of our dual-crossed transducer system.
Conclusions: Our results demonstrate the ability of the dual-crossed transducer system to target highly specific regions of mice brains using ultrasound stimulation. The proposed system is a valuable tool to study the complex neurological circuitry of the brain noninvasively.

Introduction

Direct brain neuromodulation offers distinct advantages compared to indirect pharmaceutical methods, which suffer from limited delivery through the blood-brain barrier (BBB), drug dependence and resistance, and low target specificity [1–3]. Currently, various direct brain stimulation modalities are clinically used to treat neurological pathologies such as Parkinson's disease

* Corresponding author. School of Electrical Engineering, Korea Advanced Institute of Science and Technology (KAIST), Daejeon, 34141, Republic of Korea.
** Corresponding author.
E-mail addresses: jykim@kbri.re.kr (J. Kim), hyunjoo.lee@kaist.ac.kr (H.J. Lee).
[1] These authors contributed equally.

https://doi.org/10.1016/j.brs.2021.01.002

(PD), Alzheimer's disease (AD), and depression. Some of the most widely explored technologies include deep brain stimulation (DBS), transcranial magnetic stimulation (TMS), and transcranial direct-current stimulation (tDCS) [4]. DBS based on electrical stimulation using implantable electrodes is clinically used for patients suffering from movement disorders, PD, dystonia, and tremors [5]. However, DBS requires highly invasive neurosurgical operations to implant electrodes deep within the brain and thus, is subject to low patient compliance. In contrary, TMS and tDCS are noninvasive with high patient compliance, but are limited by low spatial resolution and limited target depth [6].

Recently, a new modality based on ultrasound (transcranial focused ultrasound stimulation, tFUS), which is also noninvasive but is theoretically capable of targeting deep brain structures with high spatial resolution has been proposed and widely explored [7–20]. Since there is yet a clinically available tool that targets deep brain structures non-invasively, tFUS is increasingly recognized as a powerful tool for noninvasive neuromodulation (Supplementary Table S1). However, despite the theoretical advantage of high spatial resolution, highly specific targeting using ultrasound neuromodulation still remains a challenge [21,22]. While ultrasound neuromodulation studies on human, non-human primates, and small animals have been widely demonstrated [23–30], due to the use of curved single-element piezoelectric ultrasound transducers with elliptical focal spots, the focal volume spanned across multiple brain sub-regions in the axial direction (*i.e.* dorsoventral direction) of the beam [31] (Fig. 1A(i), 1B(i)). This problem is especially critical for small animal experiments where brain sub-regions are in the order of a few hundred microns (Supplementary Table S2, Supplementary Fig. S1).

There have been previous attempts to reduce the focal size in order to improve the target specificity of tFUS by using modulated ultrasound waves, higher-frequency ultrasound, and beamforming arrays [21,31–33]. Increasing the center frequency of curved single-element piezoelectric ultrasound transducers reduces the focal area but only in the lateral direction; the focal area in the axial direction remains unchanged [31]. Therefore, a higher frequency ultrasound beam improves the mediolateral (ML) and anteroposterior (AP) specificity but is still limited by low dorsoventral (DV) specificity. Natural beam focusing through the use of a ring-shaped ultrasound transducer based on Micro Electro Mechanical Systems (MEMS) technology has been proposed but also suffered from low axial resolution [34–36].

The most common approach to reduce focal size is to use an array of transducers and apply phase delay to achieve beamforming. Since the axial resolution is determined by the center frequency, focal length, and aperture size, for the same frequency and focal length, a larger array is required to achieve a high axial resolution [37]. For example, for a linear array with a center frequency and focal distance of 5 MHz and 2 cm, respectively, the estimated required aperture size for the linear phased array to achieve an axial resolution of 1 mm is in the meter scale, which is impractical (Supplementary Fig. S2). Hemispherical phased arrays are able to achieve high spatial resolution in the axial direction by physically positioning a large number of array elements around the skull, however, these arrays still suffer from a relatively low axial resolution and are too bulky for small animal studies [38]. Furthermore, beamforming requires complex circuitry and a signal processing unit. Recently, a new method using optoacoustics demonstrated motor neuromodulation in mice at a submillimeter spatial resolution. However, this technique is highly invasive as it required insertion of a fiber directly into the brain [39]. Therefore, there is still a challenge to achieve high spatial resolution in the axial direction for noninvasive ultrasound neuromodulation. In addition, the solution should be low-cost and simple to be readily adapted in neuroscience laboratories.

To overcome these challenges, we propose a dual-crossed transducer system that is capable of high spatial resolution in both the lateral and axial directions (Fig. 1A(ii)-(iv)). By crossing the beams of two commercially available transducers, we were able to significantly reduce the focal size in the axial direction and the focal volume. The overlapping area of the two beams formed a new focal spot and the resulting focal area was dramatically minimized compared to that of previous works. Another important advantage of this system is that the ultrasound beam intensity required for each transducer is smaller compared to that of a single transducer. Thus, the non-target brain regions along the ultrasound beam path, which are inevitably exposed, are subject to a lower intensity. In addition, our proposed system offers a new solution that does not require expensive and complicated beamforming circuitry and signal processing unit.

Material and methods

Beam profile simulation

We used finite element analysis (FEA) to simulate the beam profile of both a single transducer and dual-crossed transducers (COMSOL Multiphysics®, MA, USA). We simulated in two dimensions (2D) to minimize the computation time. The curvature of the transducer surface was set equal to that of the 5-MHz piezoelectric transducers we used for the experiments. Then, we applied a harmonic oscillation to the transducers with a few nanometers of displacement at a frequency of 5 MHz. After simulating the beam profile of the single transducer, we positioned two transducers so that two beams crossed in-phase at the focal spot. The beam profiles of two transducers positioned at the crossing angles of 45°, 60°, and 90° were simulated (Fig. 1B(ii)-(iv)). After finding the maximum intensity at the focal spot, we defined the axial and lateral resolutions according to the FWHM in the respective directions (Fig. 1C and D). All values were normalized to that of a single transducer for comparison. Furthermore, we simulated the effects of phase differences that may exist in the actual implementation by positioning one of the transducers slightly backwards to create the phase difference. Nine phase differences were simulated for three crossing-angles (45°, 60°, and 90°) (Fig. 1G). All values were normalized by the maximum intensity of the primary focal lobe observed for the in-phase condition (ideal case).

Implementation of dual-crossed transducer system

The dual-crossed transducer system consisted of two commercially available transducers (5 MHz, diameter = 19.05 mm, focal length (F) = 38.1 mm, Hagisonic Inc., Korea) and a custom-designed fixture that held the two transducers in place at a fixed angle (Supplementary Fig. S3A). The fixture consisted of a stainless steel ruled bar with two arms attached freely on the bar: a fixed arm and a mechanically translatable arm (Sciencetown Inc., Korea). The mechanically translatable arm consisted of an xyz stage with an acrylic holder for the transducer, and both arms were fixed at a 45° angle to the bar. Two identical collimators were attached to the transducers and were filled with ultrasound coupling gel (Sanipia Inc., Korea). The distance between the two arms on the bar and the position of the mechanically translatable arm were manually adjusted to achieve precise 90° beam-crossing alignment.

For precise positioning of the focal spot of the dual-crossed transducers during *in vivo* stimulation, ultrasound beam simulations of the dual-crossed transducers were conducted with the MATLAB acoustics toolbox k-Wave and mouse skull CT data

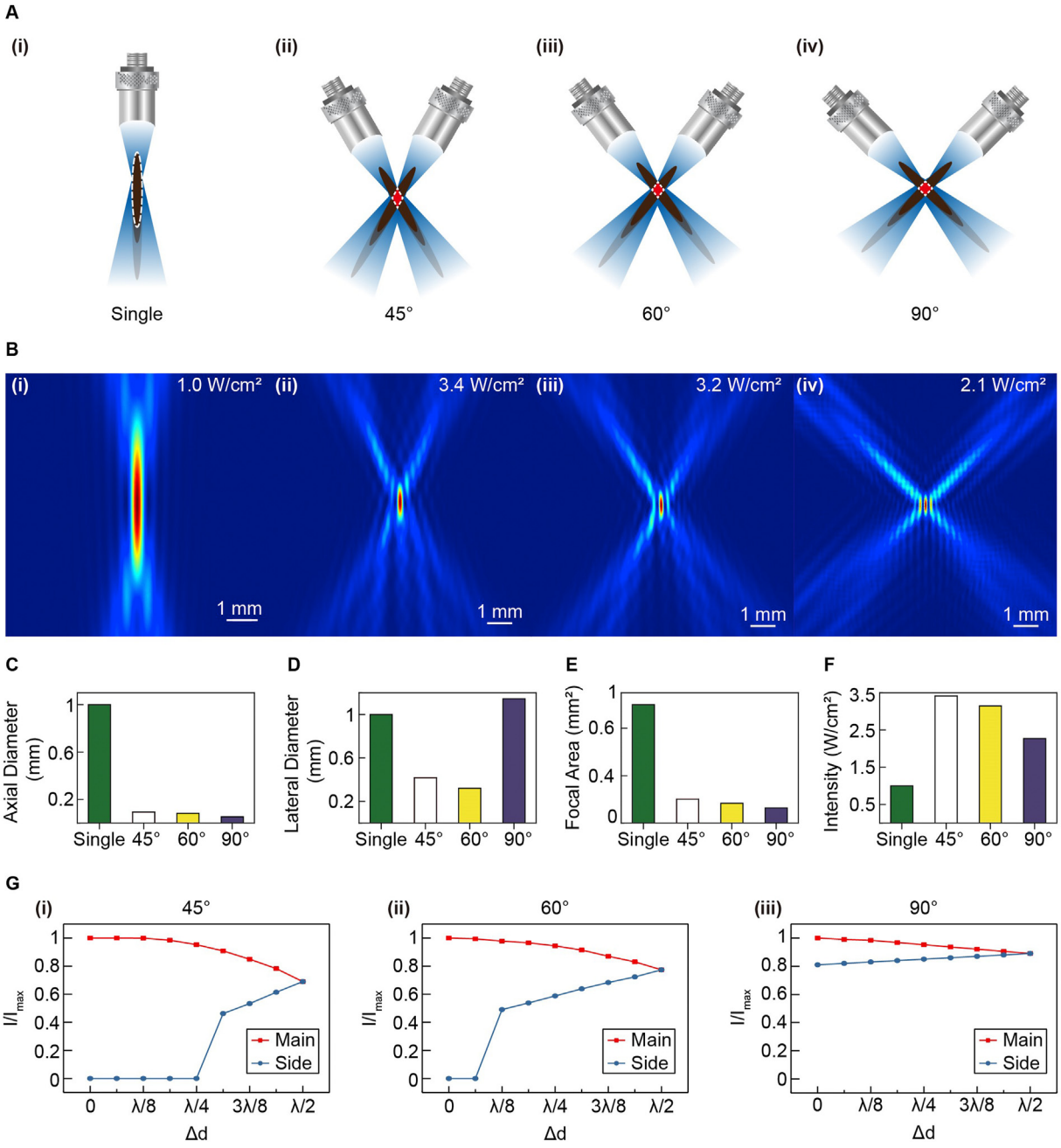

Fig. 1. Schematics and simulated beam profiles of dual-crossed ultrasound transducers with varying crossing angles. **(A)** 2D schematic of (i) a single transducer and dual-crossed ultrasound transducers with crossing angles of (ii) 45°, (iii) 60°, and (iv) 90°. **(B)** Simulated 2D ultrasound beam profiles of (i) a single transducer and dual-crossed transducers with crossing angles of (ii) 45°, (iii) 60°, and (iv) 90°. The color scale represents the relative intensity of the beam with the strongest shown in red. Normalized **(C)** axial diameter, **(D)** lateral diameter, **(E)** focal area, and **(F)** intensity to that of single transducer based on the 2D simulation results. **(G)** Normalized intensities of the primary and secondary lobes observed in the simulated beam profiles plotted against various phase differences. (For interpretation of the references to color in this figure legend, the reader is referred to the Web version of this article.)

(MathWorks®, Natick, MA, USA) [40,41]. Then, at the desired simulated brain location, the dual-transducer system was positioned using an acrylic reference needle attached to the center of the fixture bar. This reference needle was used to pinpoint the location of the bregma before stimulation to precisely position the focal spot to the known coordinates of the mouse brain (For more details on the positioning system and the custom-made MATLAB simulation program, see Supplementary Method S1). To evaluate the robustness of our custom-designed fixture, we measured the beam profile of our dual-crossed transducers after 8 months. We observed that the beam profile remained unchanged after 8 months, demonstrating the mechanical stability of our system. (For more experimental details on beam profile measurement, see Supplementary Method S2 and S3.)

In vivo animal experiment setup

All animal experiments conducted in this study were performed in accordance with protocols and ethical standards delineated by the Institutional Animal Care and Use Committee (IACUC) at the

Korea Advanced Institute of Science and Technology (KAIST, Daejeon, Korea). A total of 38 wild-type mice (C57BL/6J, 6–8 weeks old, male) were used. (For more details on surgical procedures, see Supplementary Method S1.)

In vivo neuromodulation protocol

After visual confirmation of stable breathing of anesthetized mice on the stereotaxic frame, the dual-crossed transducer system was positioned at the target region using a custom-made program that controlled the motorized stage. We applied ultrasound stimulation after 30 min of stabilization. The stimulation parameters were center frequency of 5 MHz, duration of 0.4 s, pulse repetition frequency (PRF) of 500 Hz, duty cycle of 50%, and intensity of 1 W/cm^2 (~130 mW/cm^2 accounting for skull attenuation effects) (Supplementary Fig. S3B) [31]. Using this stimulation protocol, we conducted three *in vivo* experiments to verify the functionality of our dual-crossed transducers. Specifically, we measured the success rate of motor response of the dual-crossed transducers (1) at a single coordinate with varying intensities and (2) compared with a single transducer to demonstrate the efficacy of the dual-transducer system. In addition, we observed the activation of neurons using c-Fos staining by (3) targeting the habenula, a deep-brain structure. The success rate was determined by analyzing electromyography (EMG) signals acquired from the mice's forepaw and verifying movement visually (Supplementary Fig. S3D, Supplementary Method S4). After the end of sonication, cardiac perfusion was conducted at the 30-min mark after the first ultrasound trigger was delivered. (For more details on immunohistology protocols, see Supplementary Method S5.)

For a single target region in the mouse motor cortex (ML: 0.7, AP: −0.5, DV: 1), we measured the success rate of the dual-crossed transducer system at various intensities ($n = 4$) (Supplementary Fig. S6). Then, at the same coordinates, we compared the success rate of motor responses between a single transducer and dual-crossed transducers for two cases: (1) equal single beam intensities ($n = 4$) and (2) equal focal intensities ($n = 4$). The former case confirmed the ability of the dual-crossed system to effectively use two low-powered single transducers to produce a high intensity central focal point capable of successful neuromodulation. The latter case investigated the efficacy of an improved spatial resolution for the dual-crossed system. Then, the habenula (ML: 0.2, AP: −2.1, DV: 2.4), an important deep-brain structure that is linked to depression disorder, was targeted with our dual-crossed transducer system ($n = 10$) [42]. Verification of successful stimulation of targeted regions was verified with c-Fos expression for the comparison of the single and dual-crossed transducers ($n = 16$), as well as for the stimulation of the habenula. For stimulation of the habenula, c-Fos activation was compared for (1) dual-crossed transducer stimulation of the habenula, (2) off-target stimulation of a random region (substantia nigra, ML: 1.1, AP: −2.9, DV: 4.7), and (3) no stimulation. (For more details on immunohistology protocols, see Supplementary Method S5.)

Human skull simulations

As a preliminary study, the clinical applicability of our dual-crossed transducer concept was tested with high fidelity acoustic simulations on five human head models using the Sim4Life (ZMT Zurich MedTech AG, Zurich, Switzerland) software, as described in Refs. [43,44]. We modeled the transducer as a single curved element focused transducer with a radius of curvature of 85 mm and an aperture width of 50 mm, working at a center frequency of 500 kHz, which resulted in an elliptical beam of 42 mm by 5 mm in a water background. We employed the same transducer model in all simulations and targeted the subgenual cingulate cortex (CG25), which is involved in depression [45–47]. The five human head models were taken from the multi-modal data, as described in Ref. [48]. For more details on the setup of the human skull simulations, see Supplementary Method S6.

Results

Design and working principle

In our proposed system, high axial resolution is achieved by crossing two focused ultrasound beams from commercially available piezoelectric curved transducers at the focal length of each transducer. For this scheme, the angle between two beams (*i.e.* crossing angle) is an important design parameter. Thus, we first conducted simulations using finite element analysis (FEA) to characterize the beam profile of dual-crossed transducers at varying crossing angles. Specifically, we compared the acoustic intensities of a single transducer to that of dual-crossed transducers at crossing angles of 45°, 60°, and 90°. When the two beams were crossed in-phase, the axial diameter and focal area were greatly reduced for all crossing angles (Fig. 1A and B). A crossing angle of 90° showed the highest axial resolution and doubled intensity, which were about 10 times and 2.1 times greater than that of the single transducer, respectively (Fig. 1C, F). In addition, we compared our simulation results to estimated intensity values calculated based on an analytical model that assumed in-phase condition (Supplementary Method S7). We show that it is proportional to the cosine of half the crossing angle and this value matches well with our simulation results and experimental measurements. Since the focal spot is formed through the constructive interference of two ultrasound beams, accurate alignment of two beams is critical. For example, two beams must coincide at the exact focal length of each transducer while propagating in the same plane.

However, in practice, it is difficult to achieve perfect alignment. For example, unwanted phase differences could arise due to technical errors such as minor differences in the transducers and the fixture. Thus, to assess the tolerance of our system and quantitatively analyze the effects of misalignment on intensity and spatial resolution, we simulated the performance of the dual transducers crossed at 45° and 90° at varying phases (Supplementary Fig. S4). For the crossing angle of 45°, as the phase shifts from in-phase to out-of-phase, the single primary focal lobe decreases in intensity and splits into two focal lobes (Fig. 1G(i)). We confirmed a similar phenomenon for the crossing angle of 60° (Fig. 1G(ii)). In contrary, for the crossing angle of 90°, two secondary lobes exist on both sides of the primary lobe even in the in-phase condition but this pattern does not significantly change in both intensity and shape as the misalignment worsens (Fig. 1G(iii)). Thus, while the lateral resolution of the 90°-angle case is poorer compared to the 45°-angle and 60°-angle cases due to the existence of the secondary lobes, we chose 90° for the crossing angle because of its highest axial resolution and robustness to misalignment errors (Fig. 1C,G(iii)).

Beam profile measurement of dual-crossed transducers

We custom-designed a fixture to hold two commercially available 5 MHz piezoelectric transducers that were aligned for beam crossing at a 90° angle (Supplementary Fig. S3A). First, we measured the beam profile of a single 5 MHz curved transducer to characterize the focal length (F) and FWHM (Supplementary Fig. S3C). The axial and lateral resolution defined by FWHM were approximately 10 mm and 0.8 mm, respectively. Using the focal length estimated from this measurement (F = 38.1 mm), we

adjusted our dual-transducer fixture roughly so the focal spot of each transducer crossed at 90°. For precise alignment, we iterated beam profile measurement and fixture adjustment. After a few iterations, we experimentally confirmed that the two beams were successfully aligned with a crossing angle of 90° (Fig. 2).

The center of the crossed beams formed a focal sphere with a diameter of approximately 1 mm at FWHM (Fig. 2C and D). Thus, the spatial resolution was 1 mm in both the axial and lateral directions, which matched well with our simulation results. Compared to the single transducer, we achieved a ten-fold improvement in the axial resolution using our dual-crossed transducer system. The slight increase in the lateral resolution of the dual-crossed transducers due to the secondary lobes compared to that of a single transducer was also reflected in our simulations. Moreover, similar beam patterns of primary and secondary lobes were observed to that shown in the simulation (Fig. 1B, Supplementary Fig. S4). The measured maximum intensity at the spherical focal spot of the dual-crossed transducer system was approximately double that of a single transducer, which also matched well with the simulation results (Fig. 1F). The maximum intensity of the dual-crossed transducer system was 1189 mW/cm^2, which was approximately 155 mW/cm^2 accounting for skull attenuation effects. Because of the natural increase in the intensity at the focal spot due to overlapping beams, the intensity of each ultrasound beam required for neuromodulation was smaller. Thus, using our system, non-target brain regions would be exposed to a lower intensity of ultrasound.

The skull effects of both the dual-crossed transducers and a single transducer were analyzed with beam profile measurements. We observed less beam distortion in the dual-transducers compared to that of the single transducer. In addition, intensity attenuation due to the presence of the skull was observed in both the single transducer and the dual-crossed transducer system (Supplementary Fig. S5). The intensity values were normalized by the maximum intensity measured from the dual-crossed transducers. The ultrasound beams of the single and dual-crossed transducers were reduced to 7% and 13% of its original intensity, respectively. Nonetheless, the attenuated intensity values were sufficient for noninvasive ultrasound brain stimulation [49].

Additional beam simulations including the skull effects using micro CT data of a mouse skull demonstrate the limitations of our current dual-crossed transducer system which is incapable of rotational movement. Our simulations show that the curvature of the mouse skull prevents effective beam penetration of the dual-crossed transducers as the target brain region moves away from the medio-lateral plane (Supplementary Table S3). Thus, with the current setup, stimulation of brain areas is relatively unimpeded in the antero-posterior (AP) and dorso-ventral (DV) directions but is medio-laterally (ML) confined.

In vivo animal experiments

To demonstrate the functionality of our dual-crossed transducer system, we conducted *in vivo* experiments on wild-type mice. First, the motor cortex was stimulated using the stimulation protocol that resulted in an I_{SPPA} of 1 W/cm^2 (~130 mW/cm^2 accounting for skull attenuation effects) (Supplementary Fig. S3B). Using our dual-crossed transducer system, we successfully observed induced movement in the forepaw of the mice (Movie S1). Furthermore, we measured the success rate at varying intensities. Similar to previously reported results, we observed that the success rate increased as the intensity of the dual-crossed transducer system increased (Supplementary Fig. S6, S7; $n = 4$) [35]. Thus, we demonstrated that our system was capable of neuromodulation of the motor cortex of mice.

Supplementary data related to this article can be found at https://doi.org/10.1016/j.brs.2021.01.002.

For the comparisons of induced motor responses for a single transducer against our dual-crossed transducers, we observed statistically significant (two-tailed paired *t*-test, *p < 0.05) differences in the success rates between a single transducer and our dual-crossed transducers. For the case with equal single transducer intensities, the overlapping beams of the dual transducer system allowed for more efficient stimulation with a smaller sized focus but at a higher focal intensity than the single transducer (Fig. 3A and B; Supplementary Fig. S8; $n = 4$). These results reaffirmed the intensity-dependence for successful ultrasound neuromodulation and the key advantage of our dual transducer system (*i.e.* lower intensity in the beam path and higher intensity at the target region). For the case with equal focal intensities, the success rate of eliciting a motor response was high for both the single and dual transducers, but the high resolution dual transducers demonstrated more efficient stimulation (Fig. 3D and E; Supplementary Fig. S9; $n = 4$). These results demonstrate the effectiveness of neural stimulation with the use of a high-spatial resolution dual-crossed transducer system.

c-Fos activation

Using the same protocol as the cortical stimulations, neuromodulation of the habenula, an important deep-brain structure, was conducted. Immunohistochemistry was conducted for two sets of *in vivo* experiments: (1) comparison of single vs. dual transducers, and (2) stimulation of the habenula to investigate neural tissue damage and neural activation. To quantify the neural activity with ultrasound stimulation, we performed immunohistochemistry of c-Fos, an activity dependent immediate early gene, which has been widely used as a biomarker for neural activity [50]. Mice were sacrificed and the brain was fixed with a 4% paraformaldehyde (PFA) solution at the 60 min mark after the start of ultrasound stimulation, which targeted the motor cortex and habenula. The habenula is a deep brain structure that has been suggested as a potential target region for deep brain stimulation in patients with depression [42]. Brain sections were stained with antibodies for c-Fos and DAPI and scanned with a slide scanner (Pannoramic ScanII). We analyzed the number of c-Fos positive cells in the motor/somatosensory cortex and habenula by visualizing 2D or 3D brain images using the QUINT workflow (Fig. 4A) [51–53].

DT stimulation significantly increased the number of c-Fos positive cells in the target regions compared to stimulation with a single transducer in the motor cortex (Fig. 3C,F). For the case of equal single transducer intensities, DT stimulation significantly induced more c-Fos expression compared to that of the single transducer (Fig. 3C; Supplementary Fig. S10A; $n = 8$). For the case of equal focal intensities, DT stimulation induced c-Fos expression more consistently in the target region of the motor cortex while the single transducer induced widespread cortical activity beyond the targeted motor cortex (Fig. 3F; Supplementary Fig. S10B; $n = 8$). This is consistent with the focal size of the beams as defined by the full-width half maximum intensity (FWHM). DT stimulation of the habenula significantly increased the number of c-Fos positive cells compared to DT stimulation of a random off-target region (substantia nigra, ML: 1.1, AP: −2.9, DV: 4.7) and no stimulation (Fig. 4B and C; Supplementary Fig. S10C; one-way ANOVA with Dunnett's post-hoc test, Hb: $n = 3$; off-target: $n = 3$; no-stim: $n = 4$; *p < 0.05). These results suggest efficient and target-specific neuromodulation of cortical and deep-brain regions with the dual-crossed transducer system.

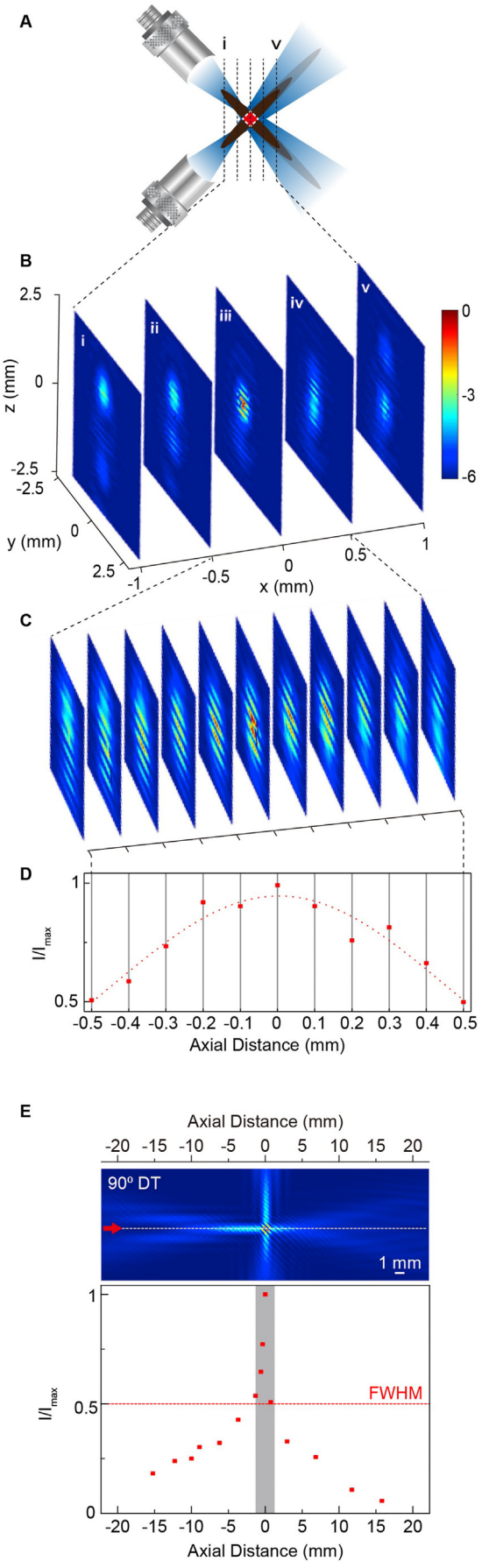

Human skull simulations

Upon verification of successful stimulation in mice, we conducted preliminary simulations to demonstrate the potential of our dual-crossed transducer concept for clinical applications in the future. To test our proposed concept on larger human brains, we conducted preliminary simulations of dual-crossed transducers in five human head models using CT and MRI data (Sim4Life, ZMT Zurich MedTech AG, Zurich, Switzerland) (Fig. 5, Supplementary Fig. S11).

The dual transducers crossed at 45° delivered a more focused intensity distribution with a better target engagement compared to a single transducer. Fig. 5A(i) and 5B(i) show the superimposition of the simulated maximum beam intensity in the brain and the anatomical T1-weighted MR image in the three planes (frontal, sagittal, and transverse) for single and dual transducers, respectively. The sagittal planes show that the ultrasonic waves from a single transducer (Fig. 5A(i)) are reflected by the base of the skull, and the maximum intensity is a few centimeters away from CG25. The transverse and frontal planes (Fig. 5A(i)) confirm that the maximum is close to the base of the skull. In contrary, the intensity beam from the dual transducers reaches the CG25 without a strong reflection pattern, and the FWHM areas (Fig. 5B(ii)) are 7.5 times smaller in the transverse and frontal planes and 2.5 smaller in the sagittal plane (Supplementary Table S4) compared to a single transducer. Finally, it is worth noting that the maximum intensity from the dual transducers is four times bigger. This is relevant for the safety of the stimulation since a lower driving pressure is needed to reach the same intensity at the target when combining two transducers [49]. In other words, the skull below the transducers and the brain areas outside the target area will absorb less acoustic energy.

Crossing angles of both 45° and 90° for the dual transducers result in high spatial resolutions. However, our simulations show that the 45° configuration results in fewer lateral side foci. Comparing the beams after cranial transmission shows that the focus region is elliptical in the sagittal planes (Supplementary Fig. S12A(i), B(i)) when the crossing angle is 45°, and more spherical when using a 90° configuration. The main difference occurs in the transverse and frontal planes (Supplementary Fig. S12A(ii, iii), B (ii, iii)), where the 90° configuration results in more lateral side foci, which can lead to unwanted side stimulations. For this reason, we chose 45° as the better configuration to target the CG25.

The similarity of the simulated beam inside the brain when targeting the CG25 with two transducers angled at 45° in five subjects confirm the stability of the approach with dual-crossed transducers in humans. Supplementary Figure S11 qualitatively shows the agreement of the simulated beams for the different head models. Quantitatively, Supplementary Table S4 shows that the FWHM areas are 14.13 ± 6.27 mm^2 (mean ± standard deviation) in the transverse plane, 17.35 ± 6.1 mm^2 in the frontal plane and 45 ± 6.13 mm^2 in the sagittal plane. The attenuation of the intensity is 7 ± 2.9%, indicating a rather high variability of the intensity that reaches the target in each head model, which suggests that

Fig. 2. Beam profile measurement of dual-crossed ultrasound transducers. **(A)** Schematic of five 2D planes selected for beam profile measurement. **(B)** Beam profile measurements of the five planes with 500 μm-steps between each plane. **(C)** Beam profile measurement of eleven planes centered at the focal spot between planes ii and iv with 100 μm-steps between each plane. **(D)** Plot of normalized intensity in the axial direction. The FWHM of the focal spot in the axial direction was 1 mm. **(E)** Axial spatial distribution of 90-crossing DT beams as a function of normalized intensity. The simulation confirms experimental beam focal size (FWHM) for entire beam crossing, including the adjacent ripples.

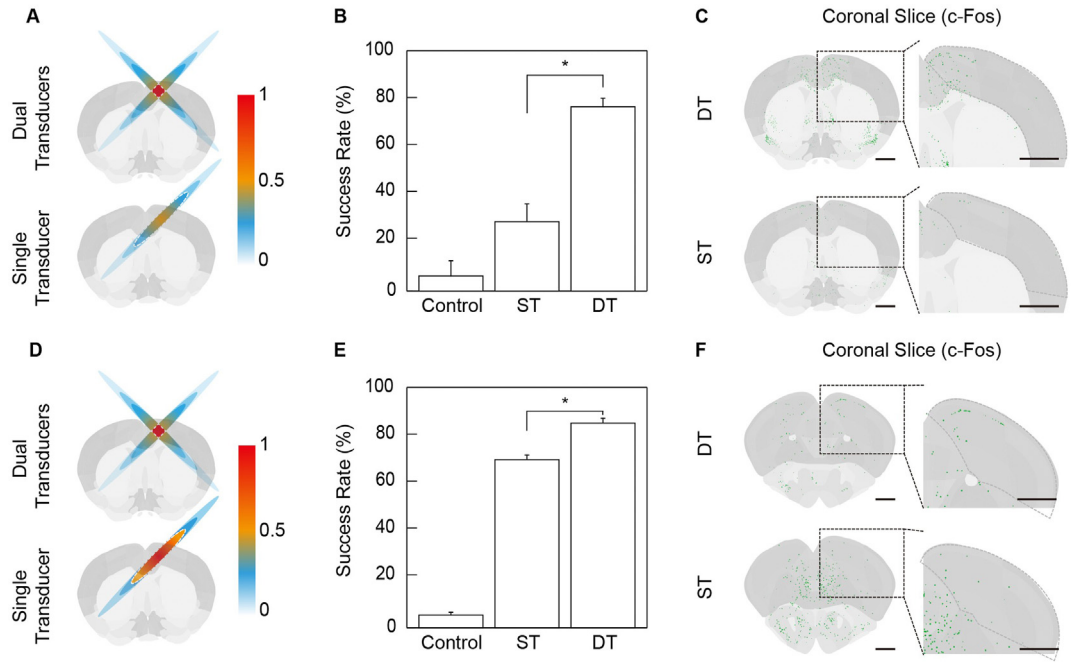

Fig. 3. Neuromodulation of motor cortex with dual and single ultrasound transducers. **(A)** Schematic of intensity profiles for the comparison between dual-crossed (DT) and single transducers (ST) for equal single beam intensities, resulting in a lower (halved) focal intensity for ST (*case 1*). **(B)** Comparison of the success rate of ultrasound stimulation between DT and ST for case 1 (equal single beam intensities, $n = 4$). **(C)** Analysis of c-Fos positive neurons for representative coronal slices of case 1 ($n = 8$). Grey dotted lines represent the motor and somatosensory areas. The black scale bar represents 1 mm. **(D)** Schematic of intensity profiles for the comparison between DT and ST for equal focal intensities, resulting in a larger focal area (FWHM) for ST (*case 2*). **(E)** Comparison of the success rate of ultrasound stimulation between DT and ST for case 2 (equal focal intensities, $n = 4$). **(F)** Analysis of c-Fos positive neurons for representative coronal slices of case 2 ($n = 8$). Grey dotted lines represent the motor and somatosensory areas. The black scale bar represents 1 mm.

individualized optimization is beneficial for accurate dose control and targeting in humans.

Using subject S1, we aimed to exemplarily demonstrate that the dual-crossed transducers enable a fine control of the focus position for individualized optimization. In Supplementary Figure S13A(i), the intensity distribution covers both the grey matter and the white matter. Slightly changing the transducer positions successfully moves the focus into grey matter of the cingulate cortex (Supplementary Fig. S13B(i)). Supplementary Figure S13A(ii), B(ii), and Table S4 confirm that the beam areas are only slightly affected (15.65 mm^2 instead of 11.02 mm^2 in the transverse plane, 15.54 mm^2 instead of 14.74 mm^2 in the frontal plane, and 51.43 mm^2 instead of 40.86 mm^2 in the sagittal plane). The attenuation of the beam is lower for the optimized position (11.1% instead of 7.39%). The latter confirms the need for individualized dose calculations.

Discussion

We successfully demonstrated an improved spatial resolution in the axial direction using our dual-crossed transducer system. An axial resolution of approximately 1 mm was achieved with our dual crossed ultrasound beams. Furthermore, we confirmed the ability of our system to stimulate millimeter-scale sub-regions of wild-type mice brains through *in vivo* experiments. This allows for targeting of neural circuit elements in small animals, which is crucial for treating various neurological pathologies noninvasively. However, we report some limitations of our proposed system: 1) bulkiness of the system, 2) potential for misalignment, 3) potential imprecise positioning of the focal spot of the dual-crossed transducers relative to the bregma, and 4) inability to accurately target medio-laterally peripheral areas of the brain. First, while our system does not require complex circuitry, its physical size is still inherently bulkier than a single transducer, which limits *in vivo* experiments to stereotaxic fixation. Second, since our system relies on the physical alignment of dual-transducer beams, the potential for misalignment depends heavily on the mechanical tolerance of the fixture. Third, the calibration procedure necessary for positioning the focal spot of the system relative to the bregma depends on the positioning of the reference needle and the step-resolution of the motorized stage, which can be subject to potential imprecision.

Fourth, simulations using the MATLAB acoustics toolbox k-Wave and micro CT data of a mouse skull have revealed limitations in targeting area due to the curvature of the skull. Our current setup uses a xyz motorized stage that can be manipulated in the 3 orthogonal axes but is incapable of rotational movement. This prevents the system from aligning the incident angle of the beams with the surface of the skull for ideal penetration in peripheral regions where the curvature of the skull becomes significant (Supplementary Table S3). Thus, our system is capable of targeting brain regions that lie within a narrow medio-lateral (ML) range but wide antero-posterior (AP) and dorso-ventral (DV) ranges. For future works with the dual-crossed transducers, an ideal setup would require a motorized stage capable of rotational movement integrated with ultrasound beam simulations of skull penetration at target brain regions.

Nonetheless, our dual-crossed transducer system presents a new high-resolution tool for ultrasound brain stimulation in small animals. The high spatial resolution of our system enables targeting of millimeter-scale sub-regional structures of small animal brains. The mice habenula, which is approximately 1 mm × 1 mm × 1.5 mm, is the perfect candidate for noninvasive tFUS using our dual-crossed transducer system. The habenula is a

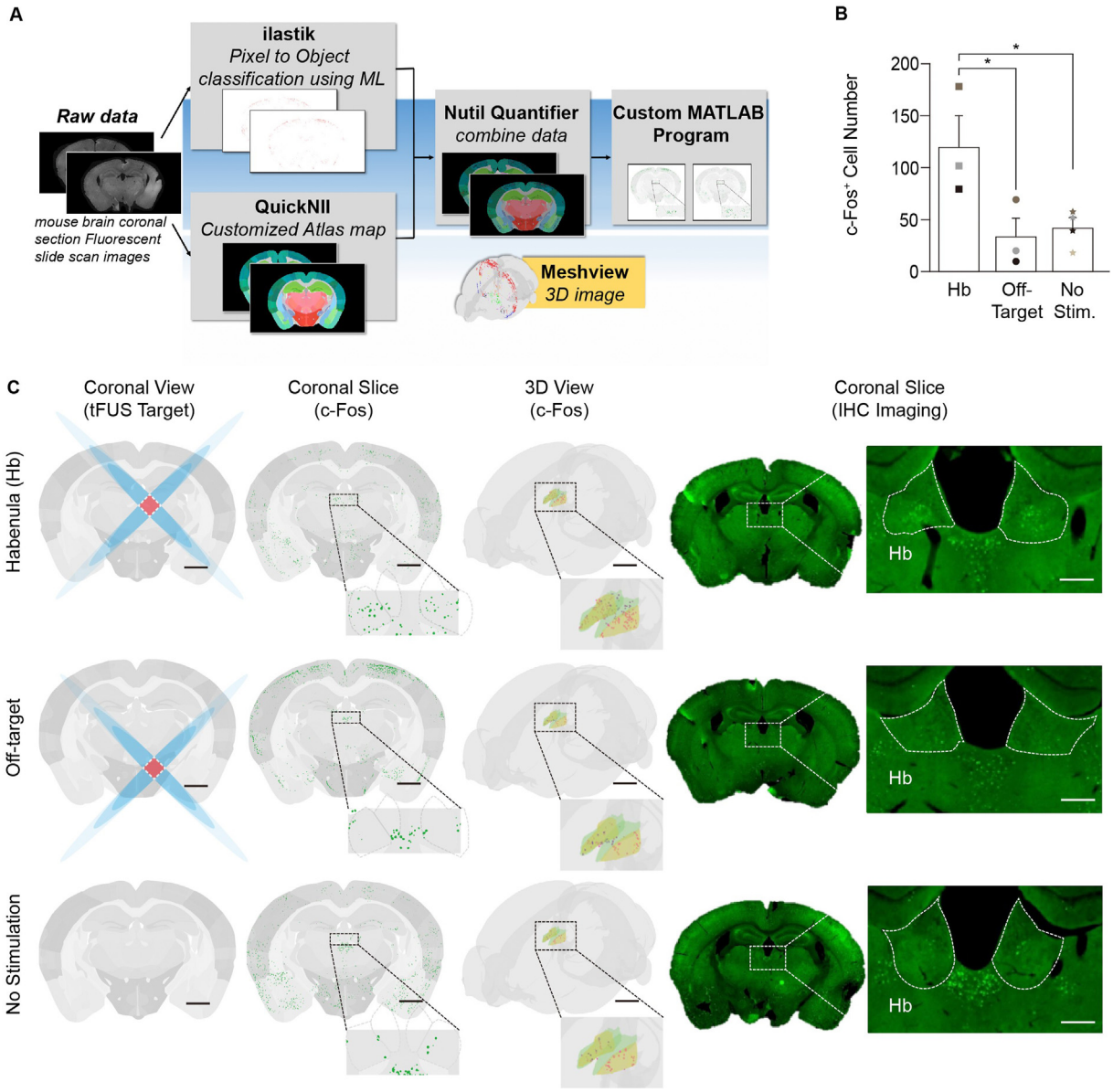

Fig. 4. Ultrasound neuromodulation of deep brain with dual-crossed ultrasound transducers. **(A)** Schematic of the QUINT workflow with custom MATLAB analysis for c-Fos activation data. **(B)** Number of c-Fos positive neurons in the habenula after DT stimulation compared with two controls: off-target stimulation and no stimulation ($n = 10$, one-way ANOVA, *$p < 0.05$). **(C)** Analysis of c-Fos staining in representative coronal slices for DT stimulation of the habenula, off-target location, and no stimulation. The black scale bar represents 1 mm and the white scale bar represents 0.25 mm for the zoomed-in IHC images.

crucial sub-region of the brain which is linked to nociception, sleep-wake cycles, reproductive behavior, and depression. Neuromodulation of the habenula and conducting subsequent behavioral *in vivo* experiments using our proposed system is a promising direction for future studies. While we demonstrated our system on small animals, which impose a challenge in terms of physical size, the concept of our dual-crossed transducers can be extended to larger animals if more rigorous modeling on beam transmission through the cranium is conducted and the positioning system is adapted for larger brains. In this study, we conducted preliminary simulations on five human head models, which demonstrated the potential for clinical applicability with our dual-crossed transducer concept.

However, an actual test of applicability is beyond the scope of this paper since the topological complexity of the human cranial surface, the variations between individual skulls (Supplementary Fig. S11, Table S4), and the wave mechanics within and without the cranial cavity require more extensive numerical modeling, simulations, and preliminary human trials. A complete acoustic model for human skull simulations does not yet exist as far as we know, and research on clinical ultrasound stimulation generally rely on partial ex-vivo skull samples and numerical simulations for accurate targeting through the cranial barrier [43,54,55]. Thus, while the concept of our system can theoretically be modified for clinical applications, significant preliminary experiments and simulations with excised skull samples would be required. In addition, a revised positioning system would be required for accurate and precise targeting of brain regions in larger and more complex brains with no standardized stereotaxic coordinate system.

Along with simulations, real-time high resolution imaging techniques such as MRI are frequently employed in conjunction with ultrasound stimulation on larger animals and humans

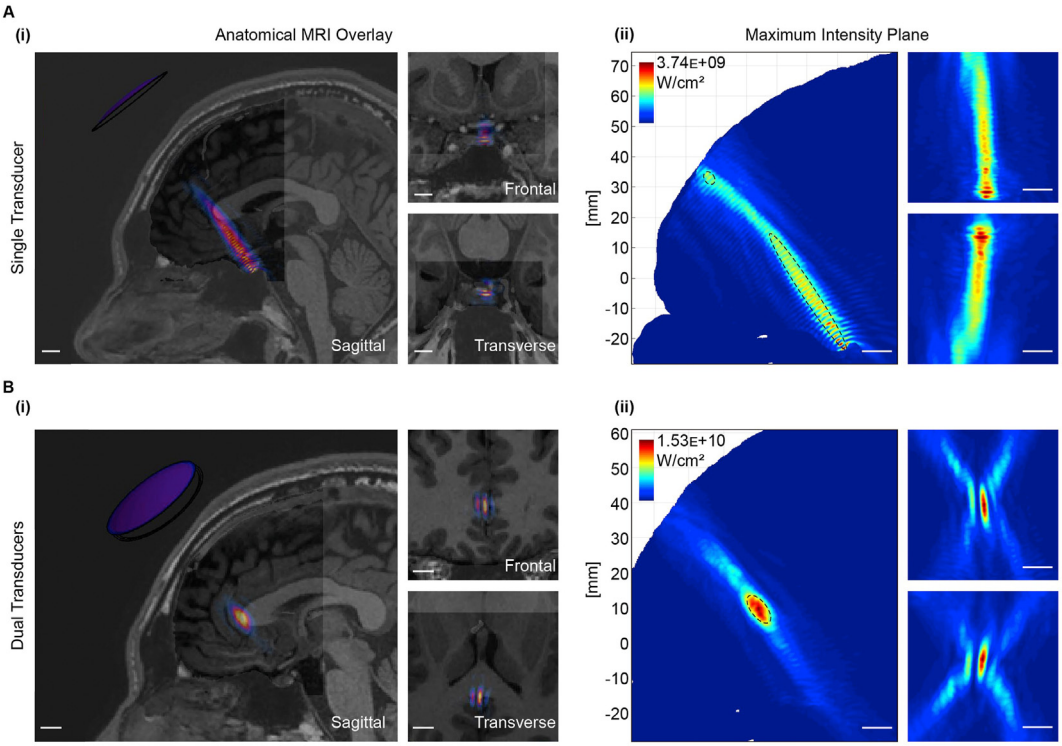

Fig. 5. Beam profile simulations for single and dual-crossed transducers in human skull. **(A)** Beam profile simulation of a single 500 kHz transducer targeting the subgenual cingulate (CG25), which is a clinically relevant brain region linked to depression. (i) Cross-sectional views of three planes, sagittal, frontal, and transverse, are shown superimposed on anatomical T1-weighted MR images, and (ii) their respective maximum intensity projections are mapped. **(B)** Beam profile simulation of dual-crossed transducers with a crossing angle of 45° and resonant frequencies of 500 kHz targeting the CG25. (i) Cross-sectional views of three planes (sagittal, frontal, and transverse) are shown superimposed on anatomical T1-weighted MR images. (ii) The maximum intensity projections are also mapped. The white scale bar represents 1 cm.

[56–58]. A recent report of ultrasound stimulation in human subjects acquired MRI scans of subjects' brains before stimulation to map the neuroanatomical structures of the brain for accurate positioning of the transducer [58]. This study also designed custom 3D-printed head-worn mounts to fix the distance of the transducer surface from the brain, and precise targeting was confirmed in real time by a two-person verification approach using a rapid scanning system calibrated with the focal length of the ultrasound beam and the relative neuroanatomical map of the brain. Our proposed system would benefit from real-time fMRI techniques for accurate positioning and targeting of brain subregions. In future works with our system, integration of MR-based imaging protocols with advanced modeling for topologically complex skulls, and improvements to the fixture system could allow for clinical applications.

Conclusions

Sub-millimeter scale targeting in wild-type mice using noninvasive ultrasound brain stimulation was demonstrated with our novel dual-crossed transducer system. Motor responses were successfully evoked in mice, and stimulation of the habenula was verified using c-Fos activation. Furthermore, as a preliminary study, the clinical applicability of the dual-crossed transducer setup was demonstrated with simulations in five human skulls targeting the subgenual cingulate cortex. This work presents a valuable biomedical tool for highly specific, noninvasive direct brain stimulation studies using tFUS in small animals with potential for clinical applications.

CRediT authorship contribution statement

Seongyeon Kim: Conceptualization, Methodology, Investigation, Writing - original draft, Visualization. **Yehhyun Jo:** Methodology, Validation, Investigation, Writing - original draft, Writing - review & editing, Visualization. **Geon Kook:** Software. **Cristina Pasquinelli:** Software, Validation. **Hyunggug Kim:** Conceptualization, Methodology. **Kipom Kim:** Investigation. **Hyang-Sook Hoe:** Methodology. **Youngshik Choe:** Methodology. **Hyewhon Rhim:** Methodology. **Axel Thielscher:** Software, Validation. **Jeongyeon Kim:** Methodology, Investigation, Formal analysis, Writing - review & editing, Visualization. **Hyunjoo Jenny Lee:** Conceptualization, Methodology, Writing - review & editing, Supervision, Project administration.

Declaration of competing interest

The authors have no potential conflicts of interest to disclose.

Acknowledgements

This research was supported by the Brain Research Program through the National Research Foundation of Korea (NRF) funded by the Ministry of Science and ICT (2016M3C7A1904343). This research was supported by KBRI basic research program through Korea Brain Research Institute funded by Ministry of Science and ICT (20-BR-02-05, 20-BR-02-15, 20-BR-03-02) and supported by the Lundbeck Foundation (grants R118-A11308 and R313-2019-622 to AT). The authors would like to thank Esra Neufeld and Hazael Montanaro for sharing the Sim4Life simulations scripts.

Appendix A. Supplementary data

Supplementary data to this article can be found online at https://doi.org/10.1016/j.brs.2021.01.002.

References

[1] Lozano AM. Waving hello to noninvasive deep-brain stimulation. N Engl J Med 2017;377(11):1096–8.
[2] Pardridge WH. The blood-brain barrier: bottleneck in brain drug development. J. Am. Soc. Exp. NeuroTherapeut. 2005;2:3–14.
[3] Ishikuro K, Dougu N, Nukui T, Yamamoto M, Nakatsuji Y, Kuroda S, et al. Effects of transcranial direct current stimulation (tDCS) over the frontal polar area on motor and executive functions in Parkinson's disease; A pilot study. Front Aging Neurosci 2018;10:231.
[4] Salling MC, Martinez D. Brain stimulation in addiction. Neuropsychopharmacology 2016;41(12):2798–809.
[5] Perlmutter JS, Mink JW. Deep brain stimulation. Annu Rev Neurosci 2006;29:229–57.
[6] Lee W, Kim HC, Jung Y, Chung YA, Song IU, Lee JH, et al. Transcranial focused ultrasound stimulation of human primary visual cortex. Sci Rep 2016;6:34026.
[7] Li X, Yang H, Yan J, Wang X, Yuan Y, Li X. Seizure control by low-intensity ultrasound in mice with temporal lobe epilepsy. Epilepsy Res 2019;154:1–7.
[8] Folloni D, Verhagen L, Mars RB, Fouragnan E, Constans C, Aubry JF, et al. Manipulation of subcortical and deep cortical activity in the primate brain using transcranial focused ultrasound stimulation. Neuron 2019;101(6):1109–11016 e5.
[9] Tyler WJ, Lani SW, Hwang GM. Ultrasonic modulation of neural circuit activity. Curr Opin Neurobiol 2018;50:222–31.
[10] Liu SH, Lai YL, Chen BL, Yang FY. Ultrasound enhances the expression of brain-derived neurotrophic factor in astrocyte through activation of TrkB-Akt and calcium-CaMK signaling pathways. Cerebr Cortex 2017;27(6):3152–60.
[11] Lee W, Lee SD, Park MY, Foley L, Purcell-Estabrook E, Kim H, et al. Image-Guided focused ultrasound-mediated regional brain stimulation in sheep. Ultrasound Med Biol 2016;42(2):459–70.
[12] Zhou H, Niu L, Meng L, Lin Z, Zou J, Xia X, et al. Noninvasive ultrasound deep brain stimulation for the treatment of Parkinson's disease modCl mouse, vol. 2019. Research (Wash D C); 2019. p. 1748489.
[13] Yoo SS, Yoon K, Croce P, Cammalleri A, Margolin RW, Lee W. Focused ultrasound brain stimulation to anesthetized rats induces long-term changes in somatosensory evoked potentials. Int J Imag Syst Technol 2018;28(2):106–12.
[14] Han S, Kim M, Kim H, Shin H, Youn I. Ketamine inhibits ultrasound stimulation-induced neuromodulation by blocking cortical neuron activity. Ultrasound Med Biol 2018;44(3):635–46.
[15] Baek H, Pahk KJ, Kim MJ, Youn I, Kim H. Modulation of cerebellar cortical plasticity using low-intensity focused ultrasound for poststroke sensorimotor function recovery. Neurorehabilitation Neural Repair 2018;32(9):777–87.
[16] Kim H, Park MA, Wang S, Chiu A, Fischer K, Yoo SS. PETCT imaging evidence of FUS-mediated (18)F-FDG uptake changes in rat brain. Med Phys 2013;40(3):033501.
[17] Kim H, Taghados SJ, Fischer K, Maeng LS, Park S, Yoo SS. Noninvasive transcranial stimulation of rat abducens nerve by focused ultrasound. Ultrasound Med Biol 2012;38(9):1568–75.
[18] Tufail Y, Matyushov A, Baldwin N, Tauchmann ML, Georges J, Yoshihiro A, et al. Transcranial pulsed ultrasound stimulates intact brain circuits. Neuron 2010;66(5):681–94.
[19] Lee W, Croce P, Margolin RW, Cammalleri A, Yoon K, Yoo SS. Transcranial focused ultrasound stimulation of motor cortical areas in freely-moving awake rats. BMC Neurosci 2018;19(1):57.
[20] Constans C, Ahnine H, Santin M, Lehericy S, Tanter M, Pouget P, et al. Non-invasive ultrasonic modulation of visual evoked response by GABA delivery through the blood brain barrier. J Contr Release 2020;318:223–31.
[21] Mehic E, Xu JM, Caler CJ, Coulson NK, Moritz CT, Mourad PD. Increased anatomical specificity of neuromodulation via modulated focused ultrasound. PLoS One 2014;9(2):e86939.
[22] Choi T, Bae S, Suh M, Park J. A soft housing needle ultrasonic transducer for focal stimulation to small animal brain. Ann Biomed Eng 2019:1–12.
[23] Deffieux T, Younan Y, Wattiez N, Tanter M, Pouget P, Aubry JF. Low-intensity focused ultrasound modulates monkey visuomotor behavior. Curr Biol 2013;23(23):2430–3.
[24] Lee W, Chung YA, Jung Y, Song IU, Yoo SS. Simultaneous acoustic stimulation of human primary and secondary somatosensory cortices using transcranial focused ultrasound. BMC Neurosci 2016;17(1):68.
[25] Kim H, Park MY, Lee SD, Lee W, Chiu A, Yoo SS. Suppression of EEG visual-evoked potentials in rats through neuromodulatory focused ultrasound. Neuroreport 2015;26(4):211–5.
[26] Pang N, Xu L, Niu L, Huang X, Zhou H, Xia X, et al. Transcranial ultrasound stimulation of hypothalamus in aging mice. IEEE Trans Ultrason Ferroelectrics Freq Contr 2020;68(1):29–37.
[27] Yuan Y, Wang Z, Liu M, Shoham S. Cortical hemodynamic responses induced by low-intensity transcranial ultrasound stimulation of mouse cortex. Neuroimage 2020:116597.
[28] Yoo SS, Bystritsky A, Lee JH, Zhang Y, Fischer K, Min BK, et al. Focused ultrasound modulates region-specific brain activity. Neuroimage 2011;56(3):1267–75.
[29] Wattiez N, Constans C, Deffieux T, Daye PM, Tanter M, Aubry JF, et al. Transcranial ultrasonic stimulation modulates single-neuron discharge in macaques performing an antisaccade task. Brain Stimul 2017;10(6):1024–31.
[30] Mueller J, Legon W, Opitz A, Sato TF, Tyler WJ. Transcranial focused ultrasound modulates intrinsic and evoked EEG dynamics. Brain Stimul 2014;7(6):900–8.
[31] Li GF, Zhao HX, Zhou H, Yan F, Wang JY, Xu CX, et al. Improved anatomical specificity of non-invasive neuro-stimulation by high frequency (5 MHz) ultrasound. Sci Rep 2016;6:24738.
[32] Kilinc MS, Aydin MA, Bozkurt A, Deveci E. Design and evaluation of phased array transducers for deep brain stimulation in nucleus accumbens region of the rat brain. In: 2017 IEEE international ultrasonics symposium (IUS). Washington, DC, USA: IEEE; 2017.
[33] Seok C, Ali Z, Yamaner FY, Sahin M, Oralkan O. Towards an untethered ultrasound beamforming system for brain stimulation in behaving animals. In: 2018 40th annual international conference of the IEEE engineering in medicine and biology society (EMBC). Honolulu, HI, USA: IEEE; 2018.
[34] Park S, Yoon I, Lee S, Kim H, Seo J-W, Chung Y, et al. CMUT-based resonant gas sensor array for VOC detection with low operating voltage. Sensor Actuator B Chem 2018;273:1556–63.
[35] Kim H, Kim S, Sim NS, Pasquinelli C, Thielscher A, Lee JH, et al. Miniature ultrasound ring array transducers for transcranial ultrasound neuromodulation of freely-moving small animals. Brain Stimul 2019;12(2):251–5.
[36] Jo Y, Oh C, Lee HJ. Microelectromechanical systems-based neurotools for non-invasive ultrasound brain stimulation. Chronobiol Med 2019;1(2):55–9.
[37] Gohari HJ. Focusing of ultrasound beams. 1997.
[38] Song J, Hynynen K. Feasibility of using lateral mode coupling method for a large scale ultrasound phased array for noninvasive transcranial therapy. IEEE Trans Biomed Eng 2010;57(1):124–33.
[39] Jiang Y, Lee HJ, Lan L, Tseng HA, Yang C, Man HY, et al. Optoacoustic brain stimulation at submillimeter spatial precision. Nat Commun 2020;11(1):881.
[40] Pichardo S, Sin VW, Hynynen K. Multi-frequency characterization of the speed of sound and attenuation coefficient for longitudinal transmission of freshly excised human skulls. Phys Med Biol 2011;56(1):219–50.
[41] Treeby BE, Jaros J, Rendell AP, Cox BT. Modeling nonlinear ultrasound propagation in heterogeneous media with power law absorption using a k-space pseudospectral method. J Acoust Soc Am 2012;131(6):4324–36.
[42] Schneider TM, Beynon C, Sartorius A, Unterberg AW, Kiening KL. Deep brain stimulation of the lateral habenular complex in treatment-resistant depression: traps and pitfalls of trajectory choice. Neurosurgery 2013;72(2 Suppl Operative):184–93. discussion ons93.
[43] Pasquinelli C, Montanaro H, Lee HJ, Hanson LG, Kim H, Kuster N, et al. Transducer modeling for accurate acoustic simulations of transcranial focused ultrasound stimulation. J Neural Eng 2020;17(4):046010.
[44] Aubry JF, Tanter M, Pernot M, Thomas JL, Fink M. Experimental demonstration of noninvasive transskull adaptive focusing based on prior computed tomography scans. J Acoust Soc Am 2003;113(1):84–93.
[45] Ge R, Downar J, Blumberger DM, Daskalakis ZJ, Vila-Rodriguez F. Functional connectivity of the anterior cingulate cortex predicts treatment outcome for rTMS in treatment-resistant depression at 3-month follow-up. Brain Stimul 2020;13(1):206–14.
[46] Connolly CG, Wu J, Ho TC, Hoeft F, Wolkowitz O, Eisendrath S, et al. Resting-state functional connectivity of subgenual anterior cingulate cortex in depressed adolescents. Biol Psychiatr 2013;74(12):898–907.
[47] Wu H, Sun H, Xu J, Wu Y, Wang C, Xiao J, et al. Changed hub and corresponding functional connectivity of subgenual anterior cingulate cortex in major depressive disorder. Front Neuroanat 2016;10:120.
[48] Silvia Farcito OP, Montanaro Hazael, Saturnino Guilherme B, Nielsen Jesper D, Madsen Camilla G, Siebner Hartwig R, Neufeld Esra, Kuster Niels, Lloyd Bryn A, Thielscher Axel. Accurate anatomical head segmentations: a data set for biomedical simulations. Berlin, Germany: EMBC; 2019. p. 6118–23. IEEE.
[49] Pasquinelli C, Hanson LG, Siebner HR, Lee HJ, Thielscher A. Safety of transcranial focused ultrasound stimulation: a systematic review of the state of knowledge from both human and animal studies. Brain Stimul 2019;12(6):1367–80.
[50] Dragunow M, Faull R. The use of c-fos as a metabolic marker in neuronal pathway tracing. J Neurosci Methods 1989;29(3):261–5.
[51] Berg S, Kutra D, Kroeger T, Straehle CN, Kausler BX, Haubold C, et al. ilastik: interactive machine learning for (bio)image analysis. Nat Methods 2019;16(12):1226–32.
[52] Yates SC, Groeneboom NE, Coello C, Lichtenthaler SF, Kuhn PH, Demuth HU, et al. QUINT: workflow for quantification and spatial analysis of features in histological images from rodent brain. Front Neuroinf 2019;13:75.
[53] Puchades MA, Csucs G, Ledergerber D, Leergaard TB, Bjaalie JG. Spatial registration of serial microscopic brain images to three-dimensional reference atlases with the QuickNII tool. PLoS One 2019;14(5):e0216796.
[54] Song J, Pulkkinen A, Huang Y, Hynynen K. Investigation of standing-wave formation in a human skull for a clinical prototype of a large-aperture, transcranial MR-guided focused ultrasound (MRgFUS) phased array: an experimental and simulation study. IEEE Trans Biomed Eng 2012;59(2):435–44.

[55] Robertson JL, Cox BT, Jaros J, Treeby BE. Accurate simulation of transcranial ultrasound propagation for ultrasonic neuromodulation and stimulation. J Acoust Soc Am 2017;141(3):1726.
[56] Ozenne V, Constans C, Bour P, Santin MD, Valabregue R, Ahnine H, et al. MRI monitoring of temperature and displacement for transcranial focus ultrasound applications. Neuroimage 2020;204:116236.
[57] Pouget P, Frey S, Ahnine H, Attali D, Claron J, Constans C, et al. Neuronavigated repetitive transcranial ultrasound stimulation induces long-lasting and reversible effects on oculomotor performance in non-human primates. Front Physiol 2020;11:1042.
[58] Badran BW, Caulfield KA, Stomberg-Firestein S, Summers PM, Dowdle LT, Savoca M, et al. Sonication of the anterior thalamus with MRI-Guided transcranial focused ultrasound (tFUS) alters pain thresholds in healthy adults: a double-blind, sham-controlled study. Brain Stimul 2020;13(6):1805–12.